Ion current rectification in funnel-shaped nanochannels: Hysteresis and inversion effects

Leon Rosentsvit, Wei Wang, Jarrod Schiffbauer, Hsueh-Chia Chang, and Gilad Yossifon

---

Articles you may be interested in

Ion current rectification in a fluidic bipolar nanochannel with smooth junction
Appl. Phys. Lett. **99**, 113103 (2011); 10.1063/1.3627181

Hysteresis of the bcc–hcp transition in a solid mixture of He 3 in He 4
Low Temp. Phys. **35**, 914 (2009); 10.1063/1.3276056

Ballistic rectification in a Z-shaped graphene nanoribbon junction
Appl. Phys. Lett. **92**, 133119 (2008); 10.1063/1.2906631

Ballistic rectification effects in InAs/AlGaSb nanostructures
AIP Conf. Proc. **893**, 577 (2007); 10.1063/1.2730023

Giant optical rectification effect in nanocarbon films
Appl. Phys. Lett. **84**, 4854 (2004); 10.1063/1.1760884

Ion current rectification in funnel-shaped nanochannels: Hysteresis and inversion effects

Leon Rosentsvit,[1] Wei Wang,[2] Jarrod Schiffbauer,[1] Hsueh-Chia Chang,[3] and Gilad Yossifon[1,a)]

[1]*Faculty of Mechanical Engineering, Micro- and Nanofluidics Laboratory, Technion—Israel Institute of Technology, Technion City 32000, Israel*
[2]*National Key Laboratory of Science and Technology on Micro/Nano Fabrication, Institute of Microelectronics, Peking University, Beijing 100871, China*
[3]*Department of Chemical and Biomolecular Engineering, Center for Microfluidics and Medical Diagnostics, University of Notre Dame, Notre Dame, Indiana 46556, USA*

Ion current rectification inversion is observed in a funnel-shaped nanochannel above a threshold voltage roughly corresponding to the under-limiting to over-limiting current transition. Previous experimental studies have examined rectification at either low-voltages (under-limiting current region) for conical nanopores/funnel-shaped nanochannels or at high-voltages (over-limiting region) for straight nanochannels with asymmetric entrances or asymmetric interfacing microchannels. The observed rectification inversion occurs because the system resistance is shifted, beyond a threshold voltage, from being controlled by intra-channel ion concentration-polarization to that controlled by external concentration-polarization. Additionally, strong hysteresis effects, due to residual concentration-polarization, manifest themselves through the dependence of the transient current rectification on voltage scan rate. © 2015 AIP Publishing LLC. [http://dx.doi.org/10.1063/1.4936915]

Ion current rectification (ICR) in a micro-nanofluidic system occurs when there is some underlying asymmetry in the system, i.e., one lateral dimension of the channel, typically of nanoscale, exhibits either a geometric or surface charge asymmetry along the axis of the ion current flux. Rectification due to geometric asymmetry has been studied using either conical nanopores[1–5] or funnel-shaped nanochannels.[6,7] As was previously shown, ion current rectification in nanochannels with uniform surface properties can result from asymmetric geometry which produces asymmetric electric-double-layers (EDLs)[1–5] along the channel. Preferential ion transport in the EDLs is responsible for both enhanced nanochannel conductance[8] and ion-perm-selectivity, wherein counterion transport is favored over that of coions due to the partial exclusion of the latter.

For slender conic nanopores, cross-sectional electro-neutrality stipulates that the concentration of the mobile ions increases towards the tip, as the total bound surface charge scales linearly with respect to the local pore radius, whereas the equal number of mobile charges is spread over the entire area which scales as the pore radius squared. This longitudinal ionic strength gradient of the mobile ions creates both a bulk conductivity gradient and a gradient in the EDL thickness. Both conspire to produce a gradient in longitudinal counterion transference number which can cause intra-channel depletion or enrichment with different pore conductance (current rectification) under opposite voltage biases.[9] The same mechanism applies for the depletion-enrichment observed[10–12] outside a straight nanochannel due

to the jump in the counterion transference number at the microchannel-nanochannel interfaces. But, when combined with an asymmetric field focusing effect at the opposite nanochannel entrances, the rectification factor is inverted with respect to the internal depletion/enrichment mechanism. Hence, there is a rectification inversion beyond a critical bulk ionic strength or voltage.[9,13–15]

Nanochannels have been shown to exhibit over-limiting currents[16] at sufficiently high voltages, wherein the current density exceeds the limiting current density predicted by the classical diffusion-limited current transport theory.[17] Below the critical voltage for this over-limiting current, the current-voltage (I-V) curve assumes a pseudo linear (ohmic) relationship. Furthermore, an electro-neutral diffusion region with an ion concentration gradient appears near the nanochannel entrance to enhance the flux via diffusion. This diffusive-flux enhanced current density begins to saturate as the electroneutral salt concentration approaches zero at the entrance of the nanochannel. At higher voltages, an extended space charge layer (SCL) much thicker than the EDL can appear[18] between the latter and the electro-neutral diffusion layer (DL) to sustain the over-limiting current density. Beyond a critical voltage threshold, electroconvective instability can occur. This selects a much shorter depletion layer length, hence, resulting in a sudden decrease of the differential resistance[19,20] to contribute to the over-limiting current. It is worth noting that in addition to electroconvective instability, both non-uniform flow due to electroosmotic flow (EOF) of the first kind and enhanced surface conduction through the quasi-equilibrium EDLs can contribute to the over-limiting current.[21] Most of the previous studies of current rectification due to gradient in EDL thickness are in the low-voltage

---

a)Author to whom correspondence should be addressed. Electronic mail: yossifon@technion.ac.il
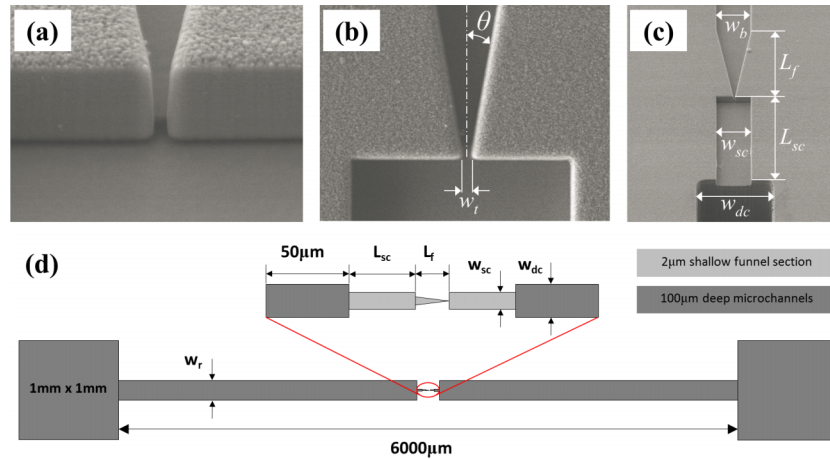
FIG. 1. SEM images of funnel-shaped nanochannel device showing: (a) close up of the narrow entrance (tip) of a single nano-funnel; (b) top view close up of the entire nano-funnel including the adjacent microchannel (from the tip-side); (c) top view of a nano-funnel, including a shallow microchannel ($w_{sc} = 10\ \mu$m and 2 μm deep) and a deep microchannel ($w_{dc} = 20\ \mu$m and 100 μm deep) leading to a wider deep microchannel (see Fig. S1(b) in the supplementary material[25]) and eventually to the reservoir; (d) top view scheme of the entire device consisting of the shallow midsection and the adjoining dark shaded deeper microchannels which lead to the reservoirs. These connecting long microchannels were made deeper in order for the funnel section to dominate the overall resistance (the resistance of the shallow midsection is about an order of magnitude larger than that of the connecting deep microchannels). Thus, enabling to sense the effect of the funnel on the ionic current rectification.

under-limiting current region.[1–7] In this under-limiting region, the ion current rectification is always in the same direction, such that the larger current is obtained when counterions are driven electrophoretically from the tip to the base of the funnel/pore. Rectification inversion at higher voltages, however, has never been verified experimentally even though it has been predicted both numerically[13–15] and theoretically.[9]

There are several indirect indications[22,23] suggesting that a current rectification reversal may occur when shifting from low-voltage (under-limiting) to high-voltage (over-limiting) currents for any asymmetric nanochannel. The small cross-sectional area of the pore/channel compared to the cross-sectional area of the same flux tube outside the pore enhances intra-pore resistance to ion current. However, once the ions are depleted at the nanochannel anodic entrance (for negatively charged walls) and a SCL develops, corresponding to over-limiting conditions, the controlling resistance shifts from the intra-pore to the depletion layer. Hence, while intra-channel ion concentration-polarization (ICP) determines the direction of the current rectification in the low voltage under-limiting current region, it is the depleted region outside the nanochannel that controls the rectification direction at the over-limiting current region at high voltages. Jung et al.[22] have demonstrated the latter over-limiting current

rectification behavior for asymmetric microchannel chambers across a cylindrical nanopore, while Yossifon et al.[23] have demonstrated it using asymmetric nanochannel entrance geometry, but symmetric intra-channel geometry, uniform EDL thickness, and symmetric opposing microchambers. Extrapolation of these findings to a conical nanopore/funnel-shaped nanochannel with symmetric microchambers suggests that, under the over-limiting conditions, the rectification direction should reverse such that higher currents would occur when the counterions transport from the base to the tip. We report here the first direct experimental verification of this rectification inversion phenomenon.

In contrast to the well-studied track-etched nanopores, we used a two-dimensional funnel-shaped nanochannel. This is advantageous because it offers far better control over the geometry and dimensions and also enables optical observation of the device to confirm the intra-channel and external ion depletion-enrichment phenomena responsible for current rectification. In contrast to Perry et al.[6,7] who used e-beam lithography to create nanometric scale funnel geometry, we used etch-deposition techniques[24] to create funnel-shaped nanochannels (Fig. 1) connected to shallow microchannels (2 μm deep) at their opposite ends. The funnel is 2 μm deep, L_f = 2.8–57 μm long with tip and base

TABLE I. Nominal geometric dimensions, X_{tip}, X_{base}, and ICR inversion voltage values of the various funnel configurations tested/simulated. The width and length of the shallow microchannels adjacent to the funnel section in the model are $w_{sc} = 10\ \mu$m and $L_{sc} = 14\ \mu$m, respectively (Fig. S2[25]).

	Funnel configuration	θ half-cone angle (deg)	L_f (μm)	L_{sc} (μm)	w_b (μm)	w_t (nm)	X_{tip}	X_{base}	V_{inv} inversion voltage (V)
Experiments	5 large	5	57	~19	10	192	36	0.7	1.40
($c_0 \approx 30\ \mu$M; $\sigma_s \approx -10$ mC/m^2)	10 small	10	2.8	~46	1	350	20	6.9	1.18
	10 large	10	30	~33	10	398	17	0.7	1.24
	20 med	20	6.8	~44	5	450	15	1.4	0.90
COMSOL	5 med	5	28.5	14	5	300	28	1.7	2.25
($c_0 = 1\ \mu$M; $\sigma_s = -0.4$ mC/m^2)	10 med	10	14	14	5	300	28	1.7	1.50
	20 med	20	6.8	14	5	300	28	1.7	1.20

widths of w_t = 190–450 nm and w_b = 1–10 μm, respectively, as detailed in Table I and in the supplementary material (Fig. S1[25]). A thick (~3 mm) PDMS (polydimethylsiloxane, SYLGARD184, Dow Corning) layer, with perforations to be used as reservoirs, was plasma bonded on top of the 100 μm rectangular DRIE (deep reactive-ion etching) etched openings in the Si layer wherein platinum or Ag/AgCl electrodes (0.5 mm in diameter) were introduced. We used a dilute potassium-chloride (KCl) solution with measured conductivity of 4-5 μS/cm, pH = 5.6-5.7 at room temperature of 25 °C in order to increase the degree of EDL overlap at the funnel tip. A GAMRY Reference 3000 potentiostat was used for the electrical measurements. For visualization of the polarized regions, we added ~10 μM of rhodamine 6G fluorescent dye to the electrolyte solution and used a Nikon Eclipse Ti confocal microscope with an Andor iXon3 camera.

The intra-funnel concentration-polarization is confirmed in Fig. 2 for various electric field intensities and polarities values. Specifically, intra-funnel ion enrichment and depletion were obtained, as expected, for a cathodic and anodic funnel base, respectively (see also movies 1 and 2 in the supplementary material[25]). Also, the intensity of the concentration-polarization increased with increasing voltage. Interestingly, the depletion layer propagated through the entire microchannel length (of depth ~100 μm) towards the anode.

In steady state/transient electrical measurement experiments, the working electrode was at the base/tip of the funnel at the applied voltage V_0, and the counter electrode was at the tip/base of the funnel held at 0 V, respectively. After a thorough cleaning procedure the chronoamperometric response of the system was measured. The current obtained after the system reached steady-state conditions (~2000 s; see Fig. S6 in supplementary material)[25] was used for extraction of the rectification factor. This is defined as $ICR = |I_{V_0<0}| / |I_{V_0>0}|$,
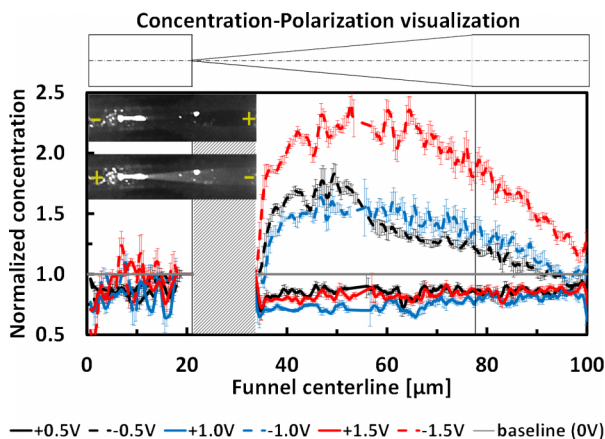

FIG. 3. Experimentally measured steady-state (~2000 s) (a) ion current rectification, $ICR = I_-/I_+$ and (b) current versus applied voltage for various funnel geometries (Table I) with ~30 μM KCl solution sampling time = 2000 s. The error bars stem from measurement-to-measurement drift and instrumentation (Gamry 3000) measurement error at low currents.

i.e., the ratio of the resulting ion currents through the system for biases with the same magnitude but opposite sign.

The results of the rectification factor versus applied voltage, *ICR-V* curve, for various funnel geometries (Table I) are depicted in Fig. 3(a). The most significant and robust observation is the appearance of a maximum in the *ICR-V* curves followed by rectification inversion ($ICR < 1$) indifferent to the funnel geometry and/or type of electrodes. The rectification effect in general and these curious features are related to EDL overlap at the tip of the funnel. This is verified with an electrolyte of higher concentration (~50 times more concentrated) wherein the rectification factor flattens to unity, indicative of its vanishing with diminishing EDL overlap.

These experimentally observed effects are in qualitative agreement with 2D numerical simulation results shown in Fig. 4 (numerical simulation details are described in the supplementary material[25]) and in Yan *et al.*[9] For the low-voltage regime (see inset of Fig. 3(b)), the current rectification direction is such that higher current is obtained when the anode is located at the tip of the funnel ($V_0 < 0$). As noted by earlier researchers, the underlying mechanism is ICP across the funnel ion-permselective tip[13,14] where the EDL overlap occurs. As usual for negatively charged walls, the depleted region is on the anodic side while the enrichment region is on the cathodic side. For $V_0 > 0$, the depletion occurs within the nanochannel while for $V_0 < 0$ it is an enrichment, in agreement with the experimental results shown in Fig. 2.

FIG. 2. Fluorescent imaging of rhodamine 6G dye mirroring the ion concentration-polarization of the background electrolyte (~30 μM KCl) within the "5 large" funnel configuration for various applied voltages after a 1000 s priming. The distribution of the normalized concentration along the funnel centerline was obtained by normalizing the local fluorescence intensity by its initial equilibrium value (3 points moving average with error bars are shown). The normalized concentration distribution was omitted from the pattern filled area, close to the funnel tip, due to local fluorescent contamination which prevented quantification. Inset corresponds to an applied voltage of 1.5 V.
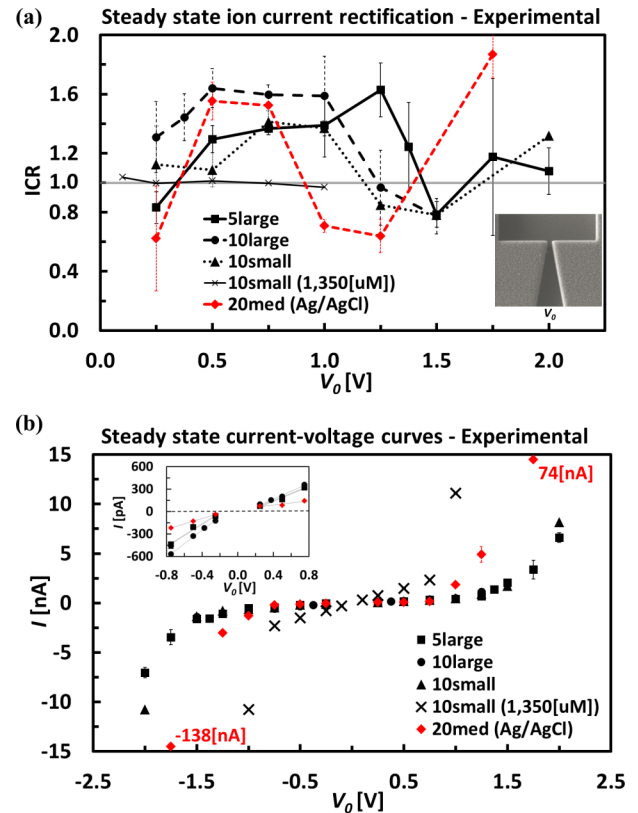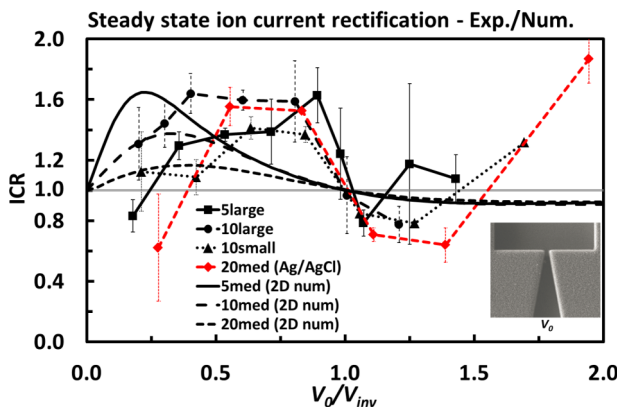
FIG. 4. COMSOL numerical steady state simulation *ICR-V* response for 5 med/10 med/20 med configurations compared to the experimental *ICR-V* response from Fig. 3(a) with the applied voltage normalized by the inversion voltage of each curve (Table I).

This corresponds to a respective decrease and increase of the ionic conductivity and an opposite trend for the overall resistance.

The voltage threshold at which the rectification inversion occurs corresponds roughly to an under-limiting to over-limiting current regime transition that is seen in the I-V response of the funnel (Fig. S4 in supplementary material[25]). Following Yan *et al.*[9] we can estimate the dimensionless parameter $X = 2\sigma_s/(zFc_0w)$ that represents the density of the surface charge, extrapolated over the funnel cross section, and is a good measure of its ion-selectivity. Herein F is the Faraday constant, z is the valency, c_0 is the electrolyte bulk concentration, σ_s is the surface charge density, and w is the local funnel cross section width. For a typical value of $\sigma_s \sim O\left(0.01\frac{C}{m^2}\right)$, the examined electrolyte concentration $c_0 \approx 3 \cdot 10^{-5}$ M and 192 nm $< w_{tip} <$ 450 nm (Table I) one obtains $X_{tip} > 10$. Hence, a qualitative agreement is obtained between our experiments (Fig. 3(a)) of the rectification inversion and the numerical results obtained in Yan *et al.*[9] (their Fig. 4(a)) in the limit of large-X. In order to facilitate the numerical simulations, due to limits on the meshing resolution, we have used smaller values for both c_0 and σ_s (see Table I) so as to increase the Debye length, which scales with the inverse square root of the concentration, and reduce numerical error stemming from the nonlinear Poisson-Boltzmann solution of the EDL. However, we have chosen the dimensionless parameters, X_{tip} and X_{base}, which are a good measure of the funnel ion-selectivity, to be on the same order of the experimental values (Table I) so as to obtain qualitatively similar current rectification response.

However, in contrast to the two-dimensional numerical simulations (Fig. 4 and Ref. 9) that predict a monotonic decrease of the rectification factor with voltage beyond the inversion point, the experiments show an abrupt increase in the rectification factor at applied voltages of ~1.25 V and ~1.5 V for Ag/AgCl and Pt electrodes, respectively. There is a considerable supporting evidence that this is associated with the onset of water electrolysis. First, the standard potential of the water electrolysis is −1.23 V at 25 °C which corresponds well with the voltage threshold seen in the Ag/AgCl electrodes setup. The increase of this threshold
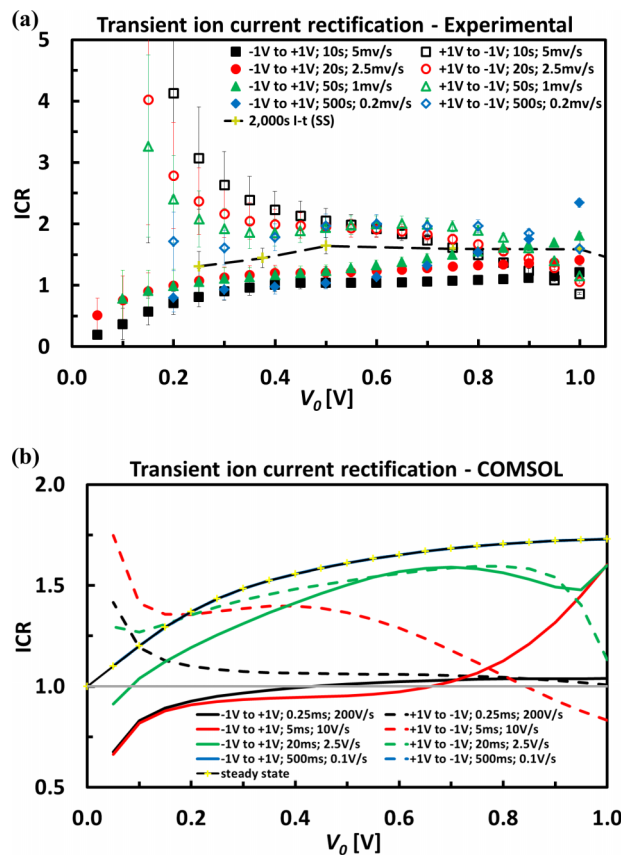

FIG. 5. (a) The experimental *ICR−V* response for various scan rates (0.2-5 mV/s; $\Delta V = 50/100$ mV; $\Delta t = 10$-500 s) and scan directions (−1 V → +1 V and *vice versa*) for "10 large" funnel configuration for ~30 μM KCl solution. A steady-state (~2000 s) ion current rectification response is also included; (b) COMSOL numerical simulation results exhibiting similar trends for "10 med" funnel configuration ($\sigma_s \sim 0.06$mC/m^2).

when using Pt instead is due to the additional voltage drop across the EDLs forming at the electrodes. In addition, the measured current dramatically increases beyond these voltages (Fig. 3(b)). Also, the emergence of bubbles at the edges of the reservoir is clearly seen at voltages beyond 5-6 V (see Fig. S5 and movie 3 in the supplementary material[25]).

Another important issue is the hysteresis effect observed when one attempts to extract the rectification factor. This stems from the residual concentration-polarization and strongly depends on the voltage scan rates. This is exhibited in the increasing difference of the measured *ICR-V* between the different scan directions with increasing scan rate (Fig. 5(a)). In contrast, in the limit of slow scan rates, the differences vanish and these two *ICR-V* collapse onto a single curve. This is in qualitative agreement with the results obtained numerically (Fig. 5(b)). Thus, the importance of performing these current rectification studies in conditions approaching steady-state is highlighted, where the dependency on the scan rate and field polarity can be discarded.

[1] Z. S. Siwy and A. Fuliński, Phys. Rev. Lett. **89**, 198103 (2002).

[2] Z. S. Siwy, Adv. Funct. Mater. **16**, 735 (2006).

[3] C. Wei, A. J. Bard, and S. W. Feldberg, Anal. Chem. **69**, 4627 (1997).

[4] P. Chen, T. Mitsui, D. B. Farmer, J. Golovchenko, R. G. Gordon, and D. Branton, Nano Lett. **4**, 1333 (2004).

[5] H. S. White and A. Bund, Langmuir **24**, 2212 (2008).

[6] J. M. Perry, K. Zhou, Z. D. Harms, and S. C. Jacobson, ACS Nano **4**, 3897 (2010).

[7] D. Hlushkou, J. M. Perry, S. C. Jacobson, and U. Tallarek, Anal. Chem. **84**, 267 (2012).

[8] D. Stein, M. Kruithof, and C. Dekker, Phys. Rev. Lett. **93**, 035901 (2004).

[9] Y. Yan, L. Wang, J. Xue, and H.-C. Chang, J. Chem. Phys. **138**, 044706 (2013).

[10] Q. Pu, J. Yun, H. Temkin, and S. Liu, Nano Lett. **4**, 1099 (2004).

[11] A. Plecis, R. B. Schoch, and P. Renaud, Nano Lett. **5**, 1147 (2005).

[12] A. Datta, S. Gangopadhyay, H. Temkin, Q. Pu, and S. Liu, Talanta **68**, 659 (2006).

[13] D. Momotenko, F. Cortés-Salazar, J. Josserand, S. Liu, Y. Shao, and H. H. Girault, Phys. Chem. Chem. Phys. **13**, 5430 (2011).

[14] D. Momotenko and H. H. Girault, J. Am. Chem. Soc. **133**, 14496 (2011).

[15] Y. Ai, M. Zhang, S. W. Joo, M. A. Cheney, and S. Qian, J. Phys. Chem. C **114**, 3883 (2010).

[16] S. J. Kim, Y.-C. Wang, J. H. Lee, H. Jang, and J. Han, Phys. Rev. Lett. **99**, 044501 (2007).

[17] V. G. Levich, *Physicochemical Hydrodynamics* (Prentice-Hall, Englewood Cliffs, NJ, 1962).

[18] I. Rubinstein and L. Shtilman, J. Chem. Soc., Faraday Trans. 2 **75**, 231 (1979).

[19] S. M. Rubinstein, G. Manukyan, A. Staicu, I. Rubinstein, B. Zaltzman, R. G. H. Lammertink, F. Mugele, and M. Wessling, Phys. Rev. Lett. **101**, 236101 (2008).

[20] G. Yossifon and H.-C. Chang, Phys. Rev. Lett. **101**, 254501 (2008).

[21] E. V. Dydek, B. Zaltzman, I. Rubinstein, D. S. Deng, A. Mani, and M. Z. Bazant, Phys. Rev. Lett. **107**, 118301 (2011).

[22] J.-Y. Jung, P. Joshi, L. Petrossian, T. J. Thornton, and J. D. Posner, Anal. Chem. **81**, 3128 (2009).

[23] G. Yossifon, Y.-C. Chang, and H.-C. Chang, Phys. Rev. Lett. **103**, 154502 (2009).

[24] F. Xie, Y. Wang, W. Wang, Z. Li, G. Yossifon, and H.-C. Chang, J. Nanosci. Nanotechnol. **10**, 7277 (2010).

[25] See supplementary material at http://dx.doi.org/10.1063/1.4936915 for videos.